




# DMSA-coated cubic iron oxide nanoparticles as potential therapeutic agents

Senem Çitoğlu<sup>1</sup> , Özlem Duyar Coşkun<sup>2</sup>, Le Duc Tung<sup>3,4</sup> , Mehmet Ali Onur<sup>5</sup> 

& Nguyen Thi Kim Thanh<sup>\*,3,4</sup> 

<sup>1</sup>Department of Nanotechnology & Nanomedicine, Institute of Science, Hacettepe University, Beytepe, Ankara, 06800, Turkey

<sup>2</sup>Thin Film Preparation and Characterization Laboratory, Department of Physics Engineering, Hacettepe University, Beytepe, Ankara, 06800, Turkey

<sup>3</sup>UCL Healthcare Biomagnetic & Nanomaterials Laboratories, The Royal Institution of Great Britain, 21 Albemarle Street, London, W1S 4BS, UK

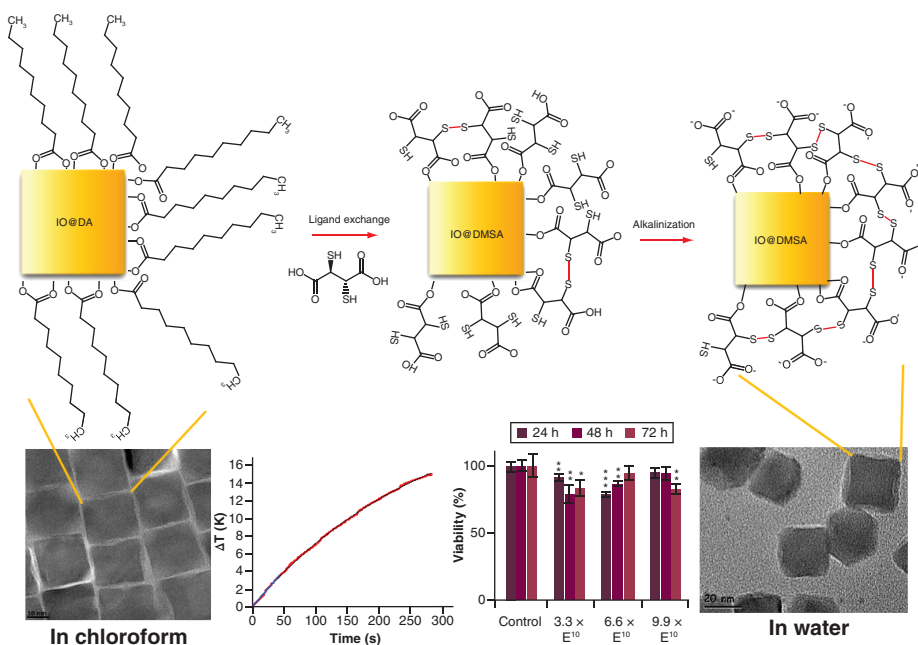
<sup>4</sup>Biophysics Group, Department of Physics & Astronomy, University College London, Gower Street, London, WC1E 6BT, UK

<sup>5</sup>Department of Biology, Faculty of Science, Hacettepe University, Beytepe, Ankara, 06800, Turkey

\*Author for correspondence: ntk.thanh@ucl.ac.uk

**Aim:** Superparamagnetic cubic iron oxide nanoparticles (IONPs) were synthesized and functionalized with meso-2,3-dimercaptosuccinic acid (DMSA) as a potential agent for cancer treatment. **Methods:** Monodisperse cubic IONPs with a high value of saturation magnetization were synthesized by thermal decomposition method and functionalized with DMSA via ligand exchange reaction, and their cytotoxic effects on HeLa cells were investigated. **Results:** DMSA functionalized cubic IONPs with an edge length of  $24.5 \pm 1.9$  nm had a specific absorption rate value of  $197.4 \text{ W/g}_{\text{Fe}}$  ( $15.95 \text{ kA/m}$  and  $488 \text{ kHz}$ ) and showed slight cytotoxicity on HeLa cells when incubated with  $3.3 \times 10^{10}$ ,  $6.6 \times 10^{10}$  and  $9.9 \times 10^{10}$  NP/mL for 24, 48 and 72 h. **Conclusion:** To the best of our knowledge, this is the first study to investigate both the cytotoxic effects of DMSA-coated cubic IONPs on HeLa cells and hyperthermia performance of these nanoparticles.

## Graphical abstract:



First draft submitted: 15 December 2020; Accepted for publication: 22 March 2021; Published online: 20 May 2021

**Keywords:** cytotoxicity • HeLa • iron oxide cubic nanoparticles • meso-2,3-dimercaptosuccinic acid (DMSA) • SAR

Future  
Medicine

Superparamagnetic iron oxide nanoparticles (IONPs) have great potential as multifunctional theranostic agents in cancer diagnosis and therapy due to their ability to be controlled magnetically toward cancer cells and that they provide contrast enhancement and generate localized heat under an alternating magnetic field (AMF). The use of magnetite ( $\text{Fe}_3\text{O}_4$ ) and maghemite ( $\text{Fe}_2\text{O}_3$ ) phases of IONPs has been clinically approved by the US FDA and the EMA [1,2]. Inside the body, IONPs are reported to be biodegradable and can be eliminated through natural metabolic pathways [3]. IONPs can be synthesized with tunable physicochemical properties (e.g., size, shape, surface charges, surface functionalities), which can affect magnetic properties, heating efficiency and blood circulation time. Under a critical size, IONPs are superparamagnetic at room temperature, having no remanent magnetization and thus substantially preventing agglomeration [4]. Their superparamagnetic property makes these nanoparticles (NPs) ideal for a wide range of biomedical applications, such as magnetically targeted controlled drug delivery, hyperthermia-induced cell death and MRI. With negligible agglomeration, the NPs can escape the reticuloendothelial system, which leads to their prolonged circulation half-life and can reduce the danger of thrombosis or blockage of blood capillaries. The heat generation capability under an external AMF is the result of Néel and Brownian relaxations, which makes these NPs potential therapeutic agents for controlled drug release and hyperthermia-induced cancer therapy [5]. For IONPs, it was reported that a short  $T_2$  relaxation time results in a darker image ( $T_2$ -weighted) and enhances MRI contrast [6]. All these properties of IONPs allow their use in the development of multiple therapeutic and diagnostic (multimodal theranostic) methods for efficient cancer diagnosis and treatment.

Although the potential of IONPs for clinical use has been approved with many formulations reaching the market [7–9], some have been later withdrawn due to safety issues related to adverse health effects [8–11], thus limiting the clinical applications of IONPs. Therefore, further formulations and extensive characterization are needed to achieve adequate simultaneous heating and image contrast for minimal NP dosage in tumor cells. Each formulation will show different magnetic behavior, heating capacity and toxicity according to the different physicochemical properties of the NPs.

Meso-2,3-dimercaptosuccinic acid (DMSA)-coated IONPs including spherical [12–23] and cubic morphologies [24–27] have been widely studied in the literature. Some of the studies [19,22,27] have only investigated hyperthermia properties of DMSA-coated IONPs, whereas others [12,14–16,18,20,21,23,24] have investigated only their cytotoxicity. In that context, some other works [13,17,25], have not even investigated either hyperthermia or cytotoxicity of such NPs. Only Kossatz *et al.* [26] studied both the hyperthermia properties and cytotoxicity of 15 nm IONPs as cores on breast and pancreatic cancer xenografts *in vivo*.

In our study, the magnetic, magnetothermal and physicochemical properties of larger (size  $\sim 24$  nm) IONPs are comprehensively investigated, as well as their cytotoxicity on HeLa cells. Here, we report the synthesis and characterization of  $\sim 24$  nm cubic DMSA functionalized IONPs. Because of their high saturation magnetization, good magnetothermal properties and nontoxicity for up to 3 days with a concentration of  $9.9 \times 10^{10}$  NP/mL *in vitro*, they can have a potential use for the multifunctional cancer diagnosis and treatment. With the size of  $< 25$  nm, it is expected that the cubic IONPs will exhibit superparamagnetism at room temperature, which is crucial for biomedical applications [11]. Compared with spherical NPs, cubes of similar size have relatively higher-ordered spins and anisotropy energy values, resulting in higher magnetization and specific absorption rate (SAR) values [28] and better  $T_2$  relaxivity [29]. The nonspherical NPs with a high-aspect ratio could also enhance blood circulation times [30]; therefore, they are subject to less bioelimination. In addition, nonspherical NPs have greater available surface area for cells to interact, which can facilitate multivalent interactions with the cell surface, resulting in higher cellular uptake compared with spherical morphology of similar size [31].

Because NPs synthesized by the thermal decomposition method are hydrophobic, a subsequent ligand exchange step will be required to make them hydrophilic for bio-applications. Here, the surface of the IONPs is modified with DMSA molecules, resulting in a stable biological ferrofluid media. The carboxylic and thiol groups of DMSA on the surface of the NPs can provide conjugation capability for drug molecules and/or targeting ligands. DMSA coating can also significantly enhance their uptake efficiency [32]. *In vitro* and *in vivo* studies have showed that cell viability and proliferation are not influenced by the DMSA coating of  $\text{Fe}_3\text{O}_4$  and  $\text{Fe}_2\text{O}_3$  NPs [32]. DMSA-coated IONPs therefore have the potential to be used as magnetic carriers to deliver high concentrations of radioisotopes to certain areas, for example, as single-photon emission computerized tomography (SPECT)/dual-modal MRI contrast agents [33].

## Materials & methods

### Chemicals

Iron(III) acetylacetonate ( $\text{Fe}(\text{acac})_3$ ,  $\geq 97\%$ ), squalene ( $\geq 95\%$ ), chloroform ( $\geq 99\%$ ), anhydrous chloroform ( $\geq 95\%$ ), acetone ( $\geq 99\%$ ), decanoic acid (DA) ( $\geq 98\%$ ), meso-2,3-dimercaptosuccinic acid (98%), toluene ( $\geq 99.7\%$ ), 3-(4,5-dimethylthiazolyl-2)-2,5-diphenyltetrazoliumbromide (MTT) ( $\geq 97.5\%$ ) and ethanol absolute were obtained from Sigma Aldrich. Dibenzyl ether (DBE), 98%, dimethyl sulfoxide ( $\geq 99\%$ ), potassium hydroxide ( $> 85\%$ ) were purchased from Merck. While phosphate-buffered saline (PBS) (Dulbecco's PBS, 1x) was obtained from Cegrogen Biotech, Roswell Park Memorial Institute (RPMI) 1640 medium (1x) was purchased from Thermo Fisher. Spectra/por float-a-lyzer with biotech cellulose ester membranes (molecular weight = 8000–10,000) were used for dialysis of DMSA-coated IONPs. All reagents were used without purification.

### Synthesis of IONPs

Synthesis of the cubic IONPs was modified from the procedure reported in the literature [34]. In our study, different surfactant concentration and different heating rates were used to obtain around 24-nm cubic IONPs. The experiments were carried out in a 50-ml three neck (29/32) round-bottom flask equipped with Allihn-type condenser. In a typical experiment, 0.353 g (1 mmol) of  $\text{Fe}(\text{acac})_3$ , 1.034 g (6 mmol) of decanoic acid (DA) were dissolved in 10 ml of squalene and 15 ml of DBE under argon flow and stirring magnetically for 25 min. The mixture was vacuumed for 5 min at room temperature and then heated to 65°C. After degassing for 120 min at 65°C, the mixture was heated to 200°C with a heating rate of 3°C/min under argon atmosphere. The reaction mixture was kept at this temperature for 2.5 h and then heated to 297°C with a heating rate of 8°C/min. On some occasions, 7°C/min and 10°C/min heating rates were also used (see [Supplementary Figures 1 & 2](#) for transmission electron microscopes [TEM] images of the obtained NPs at those heating rates). The heating rate of 8°C/min was found to be best ramp value to obtain monodisperse cubic NPs after several trials. The reaction mixture was then refluxed for 1 h at the solvent boiling temperature of  $\sim 297^\circ\text{C}$  and found to be dropping continuously throughout the reflux due to the decomposition of DBE [34]. Therefore, the set temperature during reflux was adjusted to maintain the temperature of the reaction solution and prevent polydispersity. When the reaction completed, the final black solution containing IONPs were cooled to 20°C rapidly by submerging in an ice bath to keep their shape and size intact, different from earlier synthesis reported by Guardia *et al.* [34]. After cool down, 60 ml of acetone was added to the solution, and it was centrifuged at 8500 rpm for 15 min. The supernatant was then discarded, and the black precipitate was dispersed in 3 ml of chloroform. Afterward, 60 ml of acetone was added and the obtained dispersion centrifuged at 8500 rpm for 5 min. Washing procedure with chloroform and acetone was repeated two-times more. Finally, the obtained NPs were dispersed in  $\sim 10$  ml of anhydrous chloroform and kept at 4°C.

### Synthesis of water-dispersible IONPs

Water-dispersible IONPs were obtained through the phase transfer reaction of DA-coated IONPs with DMSA, which is an anionic ligand, a good chelating agent containing two carboxylic acid and two thiol groups, adapted from the procedures reported in the literature [13,16,25]. This consisted of four main steps: ligand substitution of DA by DMSA; alkalization (or deprotonization) of the sample enhance the stability of the NPs by electrostatic repulsion between  $\text{COO}^-$  groups and increasing S-S bonds to reduce hydrodynamic size; dialysis to remove unreacted DMSA and any other small impurities present in the dispersion, such as potassium ions from potassium hydroxide (KOH) used for alkalization; and sterilization and pH adjustment to 7.4 to avoid the presence of any bacteria in the final dispersion and obtain a suitable sample for *in vitro* experiments. In the first step, in addition to the ligand exchange, a fraction of the thiol groups was oxidized to form disulphide bridges between the two DMSA molecules [27]. In the second step, the nonoxidized thiol groups and one of the DMSA carboxylic groups were deprotonated at pH = 10 with 1 M KOH solution, resulting to increase of sulfur–sulfur bonds around the NPs. This may result in better stabilization of the NPs due to the very small hydrodynamic sizes and negative charge surface. Thus, a better dispersion of IONPs at pH = 7 in aqueous media was achieved. In the following steps, alkaline NPs dispersion was purified using dialysis tubing with the molecular weight cut-off 8–10 kDa. Later, the pH of the NPs dispersion was adjusted to  $\sim 7.4$  in PBS solution and sterilized by being exposed to an ultraviolet light.

In a typical experiment, the DA-coated IONPs dispersed in chloroform were dried under vacuum and 36.2 mg of those NPs were dispersed in 18.1 ml of toluene. A solution of 33.9 mg DMSA in 1.9 ml DMSO was then added dropwise to this NP dispersion and stirred with a vortex mixer. Afterward, the mixture was sonicated for

5 min and mechanically stirred with vortex mixer at a rate of 450 rpm for 48 h at room temperature. After the reaction completed, the translucent light yellow solvent containing DA was discarded. The black particles attached to the walls of the Erlenmeyer flask were washed five-times with 20 ml of ethanol (8000 rpm, 10 min) through centrifugation to remove free DA molecules and finally redispersed in 5 ml of ultrapure water (18.2 MΩ.cm). Then, 1 M KOH was added to increase pH to 10. Resulting black homogenous dispersion was dialyzed against ultrapure water for 4 d.

### Characterization of NPs

#### Crystallographic Phase Analysis of IONPs

The crystallographic phase of the as-synthesized IONPs was examined by X-ray diffraction (XRD) measurement. Here, the IONPs dispersed in chloroform were precipitated with ethanol and dried under vacuum overnight. XRD data of the IONPs were recorded on a Panalytical X'PERT PRO MPD X-ray diffractometer using Cu K<sub>α</sub> radiation ( $\lambda = 1.540 \text{ \AA}$ ) operated at 45 kV and 40 mA with a scan range from 20 to 90 degrees and a scan step of 0.06 degrees.

#### Morphology, particle size, size distribution & elemental analyses

NPs were imaged using a FEI Tecnai G2 30 Model and JEM JEOL model 2100F TEM. These instruments were operated at an accelerating voltage of 300 and 200 kV respectively to determine the particle size and morphology. The size distribution and mean size were determined by analyzing at least 150 randomly selected NPs visualized on the different TEM images using Image-J software. Then, the polydispersity index (PDI) value was calculated by the square of the standard deviation divided by the square of the mean size of the NPs. Elemental analysis was performed by attached TEM energy dispersive X-ray (EDX) spectroscopy to verify DMSA presence by monitoring sulfur peaks corresponding to chemical composition of DMSA. Samples were prepared by placing a drop of diluted NP dispersion onto a carbon coated-copper grid (carbon film, 300 mesh Cu) and left to dry at room temperature.

#### Thermal property analysis

Thermogravimetric analysis/differential thermal analysis (TGA/DTA) experiments were carried out using TA Instruments Q600 SDT System in N<sub>2</sub> atmosphere at a heating rate of 10°C/min from room temperature to 600°C. Changes in mass due to loss of some components of the samples were recorded against temperature rise. The percentages of the magnetic contents, surfactant amounts in the as-synthesized and functionalized IONPs were determined from the experiments.

#### Magnetic characterization

Magnetic characterization of the NPs was carried out using a vibrating sample magnetometer (VSM) cryogen-free magnet system. Samples were dried in a vacuum oven before the measurements. A VSM capsule containing the powder sample was placed in the sample holder with a kapton tape. The magnetization curves were then recorded in the magnetic field range between 3 T and -3 T at a ramp rate of 0.1 T/min at room temperature.

#### Hyperthermia measurement

Magnetothermal properties of the water-dispersible IONPs (2.4 mg Fe/ml) were measured by a nB nanoscale Biomagnetics D5 series instrument under an AMF of 15.95 kA/m and frequency of 488 kHz to determine the magnetic heating efficiency.

#### Colloidal characterization

Dynamic light scattering and zeta potential measurements of the NP dispersions were performed using Malvern Zetasizer Nano ZS instrument with a 633 nm red laser and with an angle of 173 degrees between the sample and detector, being capable of both particle size analysis (hydrodynamic diameters and polydispersity index) and zeta-potential measurement for colloidal stability.

For the analyses, the DMSA-coated NPs were diluted in ultrapure water with a concentration of 0.5 mg/ml (NPs/dispersion) and the dispersion was sonicated for ~10 s before the measurements. A glass cuvette with square aperture was used. The measurements were performed in pH between 3 and 11 at 25°C with the equilibration time of 120 s. Ten millimolar KOH and 10 mM nitric acid (HNO<sub>3</sub>) solutions were used for pH adjustment. Hydrodynamic sizes and size distributions of the NPs were reported based on an average of three replicated

measurements. The number of runs per measurement was determined automatically. The mean value of number-weighted size was used similarly as reported in the literature [34] as a hydrodynamic diameter. For the zeta potential measurements, a dip cell was used. The measurements were carried out three times, with at least 10 runs in each one. The zeta potential of a NP dispersion was calculated from the average of the three readings.

### Surface chemistry characterization of IONPs

Fourier transform infrared spectroscopy (FTIR) measurements of the NPs were carried out using a Bruker VERTEX 70 spectrometer in the wavenumber range of 4000–400  $\text{cm}^{-1}$  with a resolution of 4  $\text{cm}^{-1}$  at ambient conditions. The powder samples were ground with potassium bromide (KBr) and compressed into a pellet whose spectra were recorded. KBr pellet was recorded as a reference spectrum and the reference spectrum was subtracted from the samples' spectra automatically by the Opus program.

### Iron concentration measurement

Inductively coupled plasma mass spectrometry (ICP-MS) measurements were performed using a Thermo Fisher Scientific X series 2 instrument (MA, USA) for determining the iron content of the water-dispersible NPs precisely before the cell culture experiments. After filtration with a 0.45  $\mu\text{m}$  pore size membrane filter, the samples were dissolved in 2%  $\text{HNO}_3$ . The amount of iron in the NP dilution was determined by  $^{56}\text{Fe}$  isotope measurement.

### MTT (3-(4,5-dimethylthiazolyl-2)-2,5-diphenyltetrazolium bromide) assay

To determine the number of viable cells, the formazan product was analyzed spectrophotometrically (570 nm) by a microplate reader (BMG Labtech Spectrostar Nano Absorbance Plate Reader, Ortenberg, Germany) after being dissolved in isopropanol. An increase in the viable cell number results in an increase in the amount of MTT formazan and thus an increase in the absorbance value. The absorbance results were used for determining cell viabilities and they were analyzed statistically.

### Statistical analysis

SPSS 23 software was used for statistical analysis. Shapiro–Wilk test was used for testing normality of data. The equality of variances was evaluated by Levene's test. The results of groups were compared by using the independent t-test or Mann-Whitney U-test. A p-value  $<0.05$  was considered to be statistically significant. The results were represented as the mean  $\pm$  standard deviation ( $n = 4$ ).

## Cell culture & cytotoxicity experiments

### Sample preparation

#### Filtration

Before performing the *in vitro* experiments, the NP dispersion was filtered through 45  $\mu\text{m}$  pore size polyvinylidene fluoride membrane filter. Total Fe concentration in the dispersion was calculated using the signals of  $^{56}\text{Fe}$  isotopes of ICP-MS measurements. As a final step, the pH of the dispersion was adjusted to  $\sim 7.4$  by dispersing the NPs in PBS to perform cytotoxicity experiments.

#### Sterilization

From the stock NP dispersion (108  $\mu\text{g}_{\text{Fe}}/\text{ml}$ ), diluted samples (72  $\mu\text{g}_{\text{Fe}}/\text{ml}$  and 36  $\mu\text{g}_{\text{Fe}}/\text{ml}$ ) were prepared. NPs were diluted with sterile PBS (pH 7.4, 0.1 M). Afterward, NP dispersions were exposed to UV light for 6 h. During the experiments, 10  $\mu\text{l}$  of NP dispersion was added to each well, which contained 190  $\mu\text{l}$  of culture medium for a final number of NPs per milliliter on each well of  $3.3 \times 10^{10}$ ,  $6.6 \times 10^{10}$  and  $9.9 \times 10^{10}$  (NP/ml) (details on the calculation of the number of NPs per milliliter (in one incubated well) can be found in the supplementary information, with the relevant data in Supplementary Table 1.

### Cell culture & MTT assay

HeLa cells were cultured in RPMI 1640 medium containing 10% (v/v) fetal calf serum (FCS), 1% antibiotic (streptomycin and penicillin) in 75  $\text{cm}^2$  flasks at 37°C in 5%  $\text{CO}_2$  atmosphere. Cells were seeded in 96-well plates with a concentration of 6000 cells/well and then incubated overnight. The next day, the NP dispersions with different iron concentrations (108, 72 and 36  $\mu\text{g}/\text{ml}$ ) were diluted in fresh medium in a ratio of 1:20 nanoparticle/medium and then the culture medium in the 96-well plates was replaced with 200  $\mu\text{l}$  of prepared



medium containing NPs. The plates were incubated for 24, 48 and 72 h in the incubator. After each incubation time period, the medium was removed followed by two washes with PBS. Next, 100  $\mu\text{l}$  of fresh medium containing MTT dye solution (5 mg/ml in PBS) in a ratio of 1:10 (v/v) was added to each well. After 4 h incubation at 37°C, the medium was removed. Then, 100  $\mu\text{L}$  of 2-propanol containing 0.08 M hydrochloric acid (HCl) added to each well to dissolve formazan crystals and quantified by measuring the absorbance of the solution at 570 nm by a microplate reader (BMG Labtech Spectrostar Nano Absorbance Plate Reader). The cytotoxicity was evaluated by determining the viability of HeLa cells. The viability of control HeLa cells was defined as 100% for each MTT assay. The cell viability was calculated according to following equation:

$$\text{Cell viability (\%)} = \left[ \frac{\text{Optical density}_{\text{sample}}}{\text{Optical density}_{\text{control}}} \right] \times 100\%$$

where optical density<sub>sample</sub> represents the absorbance of the wells treated with NPs and optical density<sub>control</sub> represents the absorbance from the wells untreated with NPs.

## Results

### Synthesis & physicochemical properties of IONPs

The cubic IONPs with edge length of  $24.5 \pm 1.9$  nm were synthesized by thermal decomposition method. XRD pattern of the as-synthesized IONPs showed the single phase characteristic of the iron oxide  $\text{Fe}_3\text{O}_4/\gamma\text{-Fe}_2\text{O}_3$  cubic spinel structure (see [Supplementary Figure 3](#)). Although from the XRD patterns, it is difficult to distinguish between  $\text{Fe}_3\text{O}_4$  and  $\gamma\text{-Fe}_2\text{O}_3$ , the black color of the as-synthesized NPs indicates primarily the  $\text{Fe}_3\text{O}_4$  phase. The color of the NPs gradually becomes brownish red with time during the storage suggesting the oxidation to the  $\gamma\text{-Fe}_2\text{O}_3$  phase.

TEM images of the as-synthesized IONPs are presented in [Figure 1A–C](#), which showed  $24.5 \pm 1.9$  nm ([Figure 1D](#)) cubic monodisperse NPs with a DA layer thickness of  $2.1 \pm 0.6$  nm. The formation of DA layer can be clearly seen (see [Supplementary Figure 4](#)).

The as-synthesized IONPs are hydrophobic in nature, the ligand exchange step with DMSA was required to render them dispersible in water and was carried out following similar procedures in the literature [13,16,25]. The TEM images of the hydrophilic DMSA-coated IONPs and the corresponding EDX spectrum are given in [Figure 2](#).

After the ligand exchange, the thickness of the DMSA layer was determined as  $3.5 \pm 1.4$  nm and polydispersity index value of the NPs was calculated as 0.01 indicating very narrow size distribution. The TEM images and their histogram in [Figure 2A–D](#) and the detected sulfur peak in the EDX spectrum in [Figure 2E](#), indicating the successful DMSA functionalization onto the surface of the NPs. The presence of the silicon peaks in the EDX spectrum may originate from silicon substrate on the mounting base or the old detector used.

The DMSA surface coating is also confirmed by FTIR spectroscopy by measuring pure DMSA molecules, DA-coated cubic IONPs (IO@DA) and DMSA-coated cubic IONPs (IO@DMSA), as shown in [Figure 3](#). Here, the broad bands at  $\sim 3400$   $\text{cm}^{-1}$  in the spectra of IO@DA ([Figure 3B](#)) and IO@DMSA ([Figure 3A](#)) are associated with the OH group stretching modes indicating the presence of adsorbed water molecules. The bands in the region of  $400$   $\text{cm}^{-1}$  and  $600$   $\text{cm}^{-1}$  are related to vibrations of the Fe–O bonds [17,25,35,36]. In the spectrum of IO@DA, the two sharp bands at  $2923$  and  $2855$   $\text{cm}^{-1}$  are due to asymmetric  $\text{CH}_2$  [ $\nu_{\text{as}}(\text{CH}_2)$ ] and symmetric  $\text{CH}_2$  stretching [ $\nu_{\text{s}}(\text{CH}_2)$ ] vibrations respectively [12,36,37], characteristic of  $\text{CH}_2$  chains in decanoic acid. The two bands at  $1526$  and  $1412$   $\text{cm}^{-1}$  were attributed to the asymmetric [ $\nu_{\text{as}}(\text{COO}^-)$ ] and symmetric [ $\nu_{\text{s}}(\text{COO}^-)$ ] carboxylate stretching vibrations [37,38] and indicated that decanoic acid was bound covalently to the surface of the IONPs.

The sharp peak at  $1703$   $\text{cm}^{-1}$  in the pure DMSA spectrum ([Figure 3C](#)) is attributed to the symmetric stretching of the carbonyl group C=O [12,39]. After ligand exchange, the C=O double bond peak is observed to shift at  $\sim 1400$  and  $1620$   $\text{cm}^{-1}$  due to the splitting, which correspond to symmetric and asymmetric stretching vibrations of the carboxylate ( $\text{COO}^-$ ) ions, respectively [12,13]. This is presumably due to the DMSA molecules attached to the iron oxide's surface through the  $\text{COO}^-$  group [40]. According to the previous studies [33], the interaction between the carboxylate head and the metal atom was classified as monodentate, chelating bidentate and bridging bidentate structures, and the separation ( $\Delta\nu$ ) between the wave numbers of the [ $\nu_{\text{s}}(\text{COO}^-)$ ] and [ $\nu_{\text{as}}(\text{COO}^-)$ ] infrared bands can be used to determine the type of interaction between the carboxylate groups of the DA and the iron atom. Here, the largest  $\Delta\nu$  values ( $200\text{--}320$   $\text{cm}^{-1}$ ) correspond to the monodentate structure, the smallest

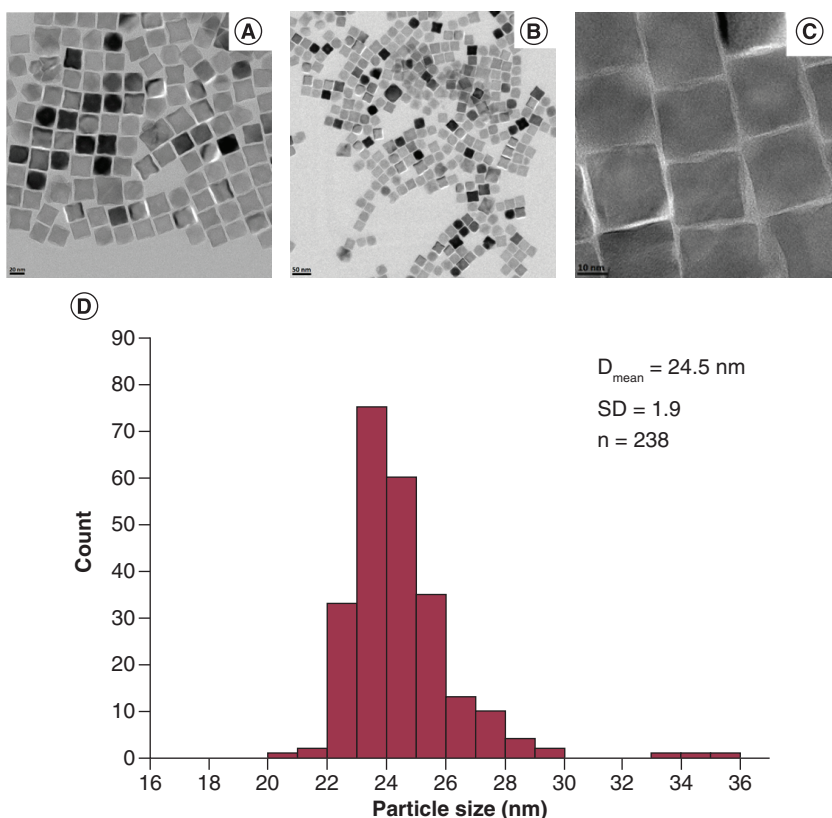


**Figure 1. Transmission electron microscope images (A–C) at different magnifications and particle size distribution (D) of the decanoic acid-coated iron oxide nanoparticles synthesized by thermal decomposition method. Scale bars for A, B and C: 20 nm, 50 nm and 10 nm, respectively.**

$D_{\text{mean}}$ : Mean cube edge length of the nanoparticles;  $n$ : Number of the nanoparticles counted; SD: Standard deviation.

$\Delta\nu$  values ( $<110\text{ cm}^{-1}$ ) the chelate bidentate structure and the medium range  $\Delta\nu$  values ( $140\text{--}190\text{ cm}^{-1}$ ) the bridging bidentate structure. The obtained separation ( $\Delta\nu$ ) between the wave numbers of the [ $\nu_s(\text{COO}^-)$ ] and [ $\nu_{\text{as}}(\text{COO}^-)$ ] infrared bands for the DMSA coated IONPs is  $215\text{ cm}^{-1}$ , which refer to the monodentate structure where one iron ion is bound to one carboxylic oxygen atom. The sharp peaks at  $2563$  and  $2538\text{ cm}^{-1}$  in DMSA spectrum (Figure 3c) could be originated from the vibrations of the thiol groups (S–H), which are absent in the spectra of the DMSA-coated IONPs, presumably due to oxidation of the thiol groups into disulfide (S–S) during ligand exchange and alkalization processes. The disulfide IR bands ( $500\text{--}540\text{ cm}^{-1}$ ) [13] could not be seen in the FTIR analysis due to the overlapping with Fe–O band or low transmittance. The absence of the two sharp bands associated with the  $\text{CH}_2$  group vibrations at  $\sim 2923$  and  $2855\text{ cm}^{-1}$  characteristic for the  $\text{CH}_2$  chains in DA [12,36,37] in the spectrum of DMSA-coated IONPs can be attributed to the nonexistence of the residual DA on the NP surfaces after the ligand exchange. Similarly, the absence of two sharp peaks at around  $1530$  and  $1415\text{ cm}^{-1}$  corresponding to the asymmetric [ $\nu_{\text{as}}(\text{COO}^-)$ ] and symmetric [ $\nu_s(\text{COO}^-)$ ] carboxylate stretching [37,38] indicating the absence of DA bound covalently to the surface of the IONPs [12,13,37,38], which supports the accomplishment of the ligand exchange process.

The coating efficiency was also examined by TGA measurements and the results are shown in Figure 4A before and after modification of IONPs with DMSA. A slight mass loss during the heating at  $140^\circ\text{C}$  in both curves (0.68% for IO@DA in Figure 4Aa, 1.12% for IO@DMSA in Figure 4Ab) is probably originated from the adsorbed water and/or residual organic solvent, chloroform. For IO@DA, a significant mass loss took place in three steps between  $140$  and  $500^\circ\text{C}$  is  $\sim 5.60\%$ , which is associated with the decomposition of organic DA molecules on the surface of the IONPs. For IO@DMSA, it also reveals three mass loss steps between  $140$  and  $500^\circ\text{C}$  corresponding to the burning of DMSA ligands on the surface of the NPs, and was  $\sim 2.35\%$ .

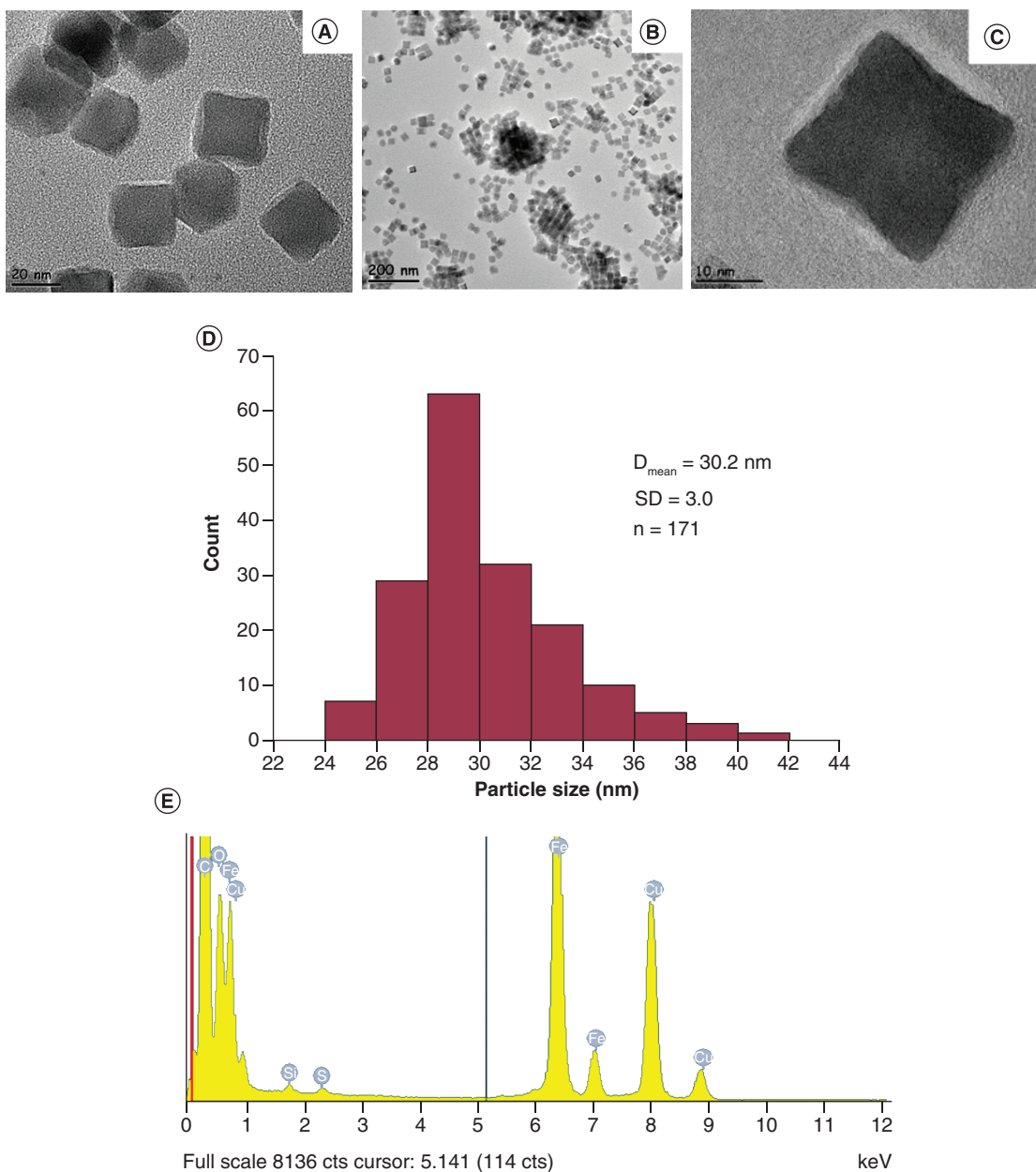


**Figure 2. Transmission electron microscope images (A–C) at different magnifications, corresponding particle size distribution (D) and transmission electron microscope energy dispersive x-ray spectrum (E) of the iron oxide nanoparticles after surface functionalization with meso-2,3-dimercaptosuccinic acid.**  
 $D_{\text{mean}}$ : Mean cube edge length of the nanoparticles;  $n$ : Number of the nanoparticles counted;  $SD$ : Standard deviation.

### Magnetization analysis

The magnetization curves of the IONPs before and after DMSA coating are presented in Figure 4B and show no hysteresis at room temperature, a characteristic of superparamagnetic behavior. Following conjugation with DMSA, the saturation magnetization is seen to increase from 74.2 to 89.6 emu/g compared with that of 92 emu/g for the bulk  $\text{Fe}_3\text{O}_4$  [13,41].

### Hydrodynamic size & colloidal stability analyses

The dynamic light scattering results of the water-dispersible IONPs given as the mean value of number-weighted size are shown in Figure 5A.



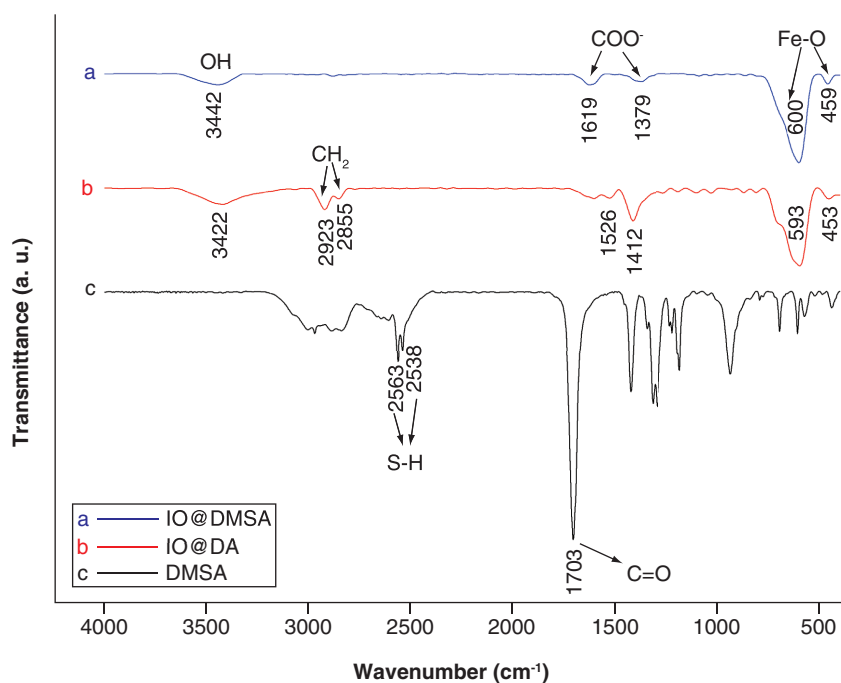


**Figure 3.** Fourier transform infrared spectroscopy spectra of meso-2,3-dimercaptosuccinic acid-coated iron oxide nanoparticles (A), decanoic acid-coated iron oxide nanoparticles (B) and pure meso-2,3-dimercaptosuccinic acid (C). DA: Decanoic acid; DMSA: Meso-2,3-dimercaptosuccinic acid; IO: Iron oxide.

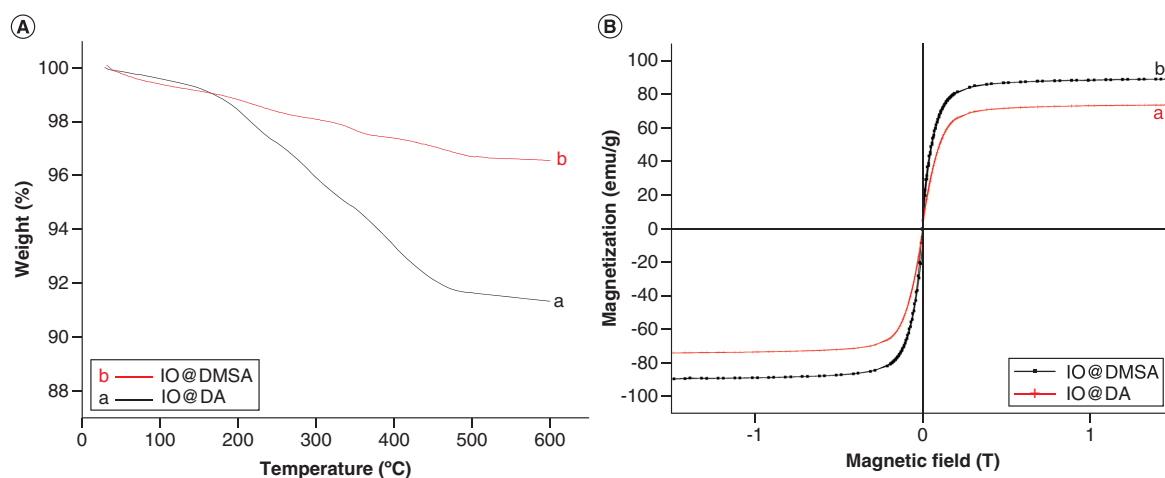


**Figure 4.** Thermogravimetric analysis curves (A) of iron oxide nanoparticles before (a) and after (b) meso-2,3-dimercaptosuccinic acid coating, and magnetization curves (B) of cubic iron oxide nanoparticles at room temperature before (a) and after (b) meso-2,3-dimercaptosuccinic acid coating. DA: Decanoic acid; DMSA: Meso-2,3-dimercaptosuccinic acid; IO: Iron oxide.

Assuming the spherical shape, the obtained hydrodynamic diameter of the IONPs at physiological pH (pH = 7.5) is  $94.0 \pm 20.1$  nm with the corresponding polydispersity index of  $0.585 \pm 0.015$ . While varying pH values from 5 to 11, the hydrodynamic diameter of the NPs does not show a significant change. The results of zeta potentials of the water-dispersible DMSA-coated IONPs as a function of pH values are presented in Figure 5B. It can be seen that at pH of  $\sim 3.5$ , the NPs have a zeta potential value less than  $-30$  mV, which is generally considered as a threshold value for the electrostatic stabilization. When the repulsive charges could not overcome the attractive Van der Waals interactions, causing agglomeration of the NPs, it will give rise to the increase in the hydrodynamic diameter within reasonable standard deviation, as seen in Figure 5A.

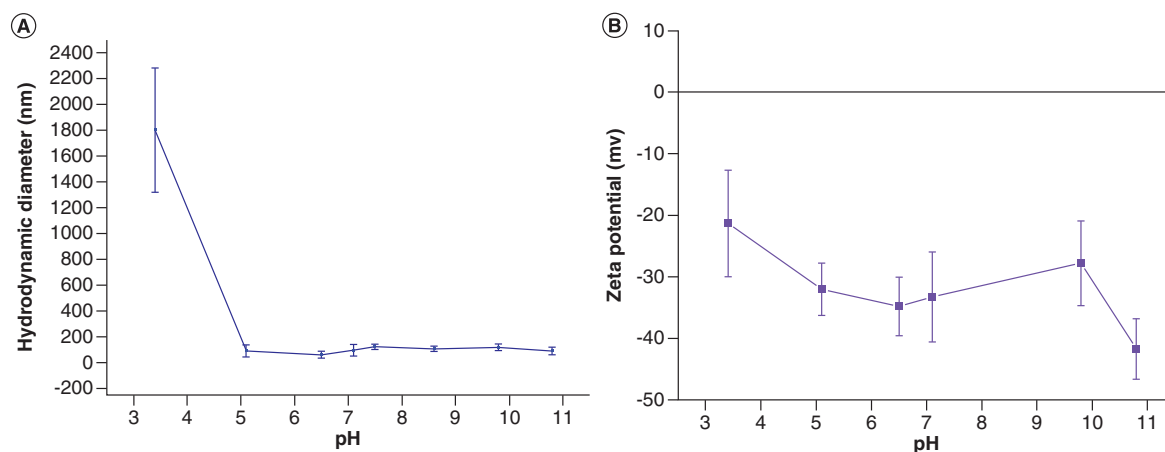


**Figure 5.** Number-weighted hydrodynamic diameters of the water-dispersible iron oxide nanoparticles (A), and the zeta potentials of the water-dispersible iron oxide nanoparticles as a function of pH values (B).

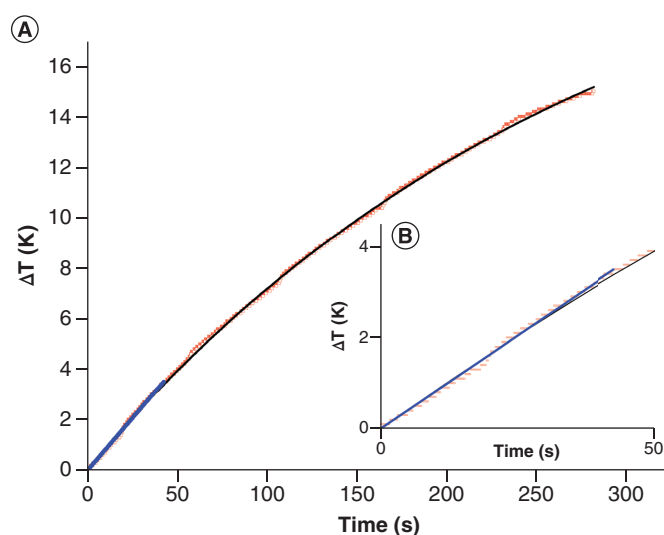


**Figure 6.** Hyperthermia result of water-dispersible meso-2,3-dimercaptosuccinic acid-coated cubic iron oxide nanoparticles (IO@DMSA; 2.4 mg Fe/ml) measured in alternating magnetic field of 15.95 kA/m and frequency of 488 kHz. (A) Temperature increase as a function of time (the red line represents the obtained data from the hyperthermia measurement, the black solid line the fit data to  $\Delta T = \Delta T_m(1 - e^{-\frac{t}{\tau}})$  function; the blue line is the linear fit showing the initial slope of the black curve at  $t = 0$ ). (B) Zoom-in view of temperature versus time curve.

The zeta potential measurements within the experimental pH range of the water-dispersible DMSA-coated IONPs showed the negative zeta potentials in between  $-21.3 \pm 8.6$  and  $-41.7 \pm 4.9$  mV, which can be attributed to the carboxyl groups of DMSA molecules. By increasing the pH value to alkaline condition, the zeta potentials of the DMSA-coated IONPs were improved. The higher the ionization, the higher the surface charge density, and the higher the electrostatic repulsion between the NPs provided by  $\text{COO}^-$  groups and thus it enhances colloidal stability. Below a pH value of 3.5, the colloidal stability was lost, and NPs began to agglomerate. In general, the solution of NPs is considered stable if the absolute value of zeta potential is larger than 30 mV. At around physiological pH (pH = 7.1), the zeta potential value of the DMSA-coated IONPs is  $-33.3 \pm 7.4$  mV and has a good colloidal stability. At pH value below 3, the DMSA-coated IONPs carry no net charge corresponding to their isoelectric point.

### Results of hyperthermia experiment

The results of the hyperthermia experiment are presented in Figure 6 with temperature increase  $\Delta T$  as a function of time. It can be seen that a temperature increase from  $22^\circ\text{C}$  to  $37^\circ\text{C}$  take approximately 5 min of AMF exposure. The SAR value determination is based on the following equation:

$$SAR = \frac{\sum_i m_i c_i}{m_{mag}} \left| \frac{d(\Delta T)}{dt} \right|_{t=0}$$

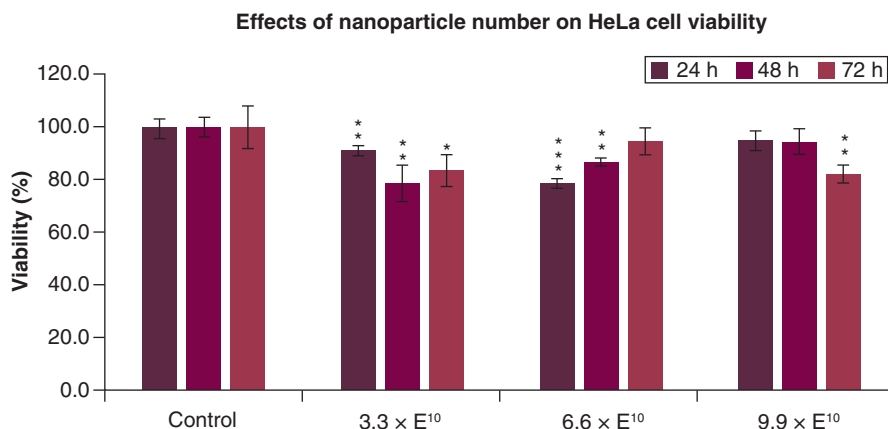


**Figure 7.** Time and nanoparticle number-dependent cell viability percentages of meso-2,3-dimercaptosuccinic acid-coated iron oxide nanoparticles according to 3-(4,5-dimethylthiazolyl-2)-2,5-diphenyltetrazolium bromide assay. All values are represented as mean  $\pm$  standard deviation. \* $p < 0.05$ ; \*\* $p < 0.01$  and \*\*\* $p < 0.001$ .

where  $m_i$  is the mass,  $c_i$  the specific heat capacity,  $m_{mag}$  the total magnetic mass and

$$|d(\Delta T)/dt|_{t=0} = \frac{\Delta T_m}{\tau}$$

the initial slope of the time-dependent heating curve.

In the calculation, it was assumed that the heat capacity of water at 22°C  $C_{water} = 4187$  J/kgK and the specific heat capacity of the magnetite  $C_{Fe_3O_4} = 651$  J/kgK [42]. The DMSA component was omitted because of its negligible mass compared with the mass of the iron oxide in coated NPs. The calculated SAR value of the IONPs normalized to the iron amount is 197.4 W/g<sub>Fe</sub> under the applied AMF.

It is well known that the calculated SAR value varies by changing the size, shape and surface coating composition in NPs. To compare hyperthermia result with the literature, intrinsic loss parameters (ILP) were calculated using the following equation:

$$ILP \text{ [nHm}^2\text{kg}^{-1}] = \frac{SAR \text{ [Wkg}^{-1}]}{f[\text{kHz}] H^2 \text{ [kAm}^{-1}]^2}$$

The ILP value for the DMSA-coated IONPs was calculated as 1.59 nHm<sup>2</sup>kg<sup>-1</sup>.

### Cytotoxicity assessment

The cell viability percentages of the DMSA-coated IONPs at different NP concentrations ( $3.3 \times 10^{10}$ ,  $6.6 \times 10^{10}$  and  $9.9 \times 10^{10}$  NP/ml) and time intervals (24, 48, 72 h) are shown in Figure 7 based on MTT assays. *In vitro* cytotoxicity assays showed that the NPs slightly affected HeLa cell viability (less than 21%) at the experimental concentrations after 24 h, 48 h and 72 h compared to the control groups. The cells remained more than 78% viable relative to the control group for all three different time periods (see Supplementary Table 2 for independent t-test and Mann Whitney U-test results).

Incubation of cells with an NP concentration of  $3.3 \times 10^{10}$  NP/ml resulted in a statistically significant change in the cell viability for all three time periods, with a minimum cell viability of  $78.6 \pm 6.8\%$  (for the lowest NP concentration after 48 h and  $6.6 \times 10^{10}$  NP/ml after 24 h). For the NP concentration of  $6.6 \times 10^{10}$  NP/ml, a statistically significant change in the cell viability was observed in the first two time periods studied, in contrast to the one after 72 h with the same NP concentration. The NPs with a concentration of  $9.9 \times 10^{10}$  did not cause a significant change in the cell viability within 48 h; however, it reduced the cell viability to  $82.3 \pm 3.4\%$  after 72 h.

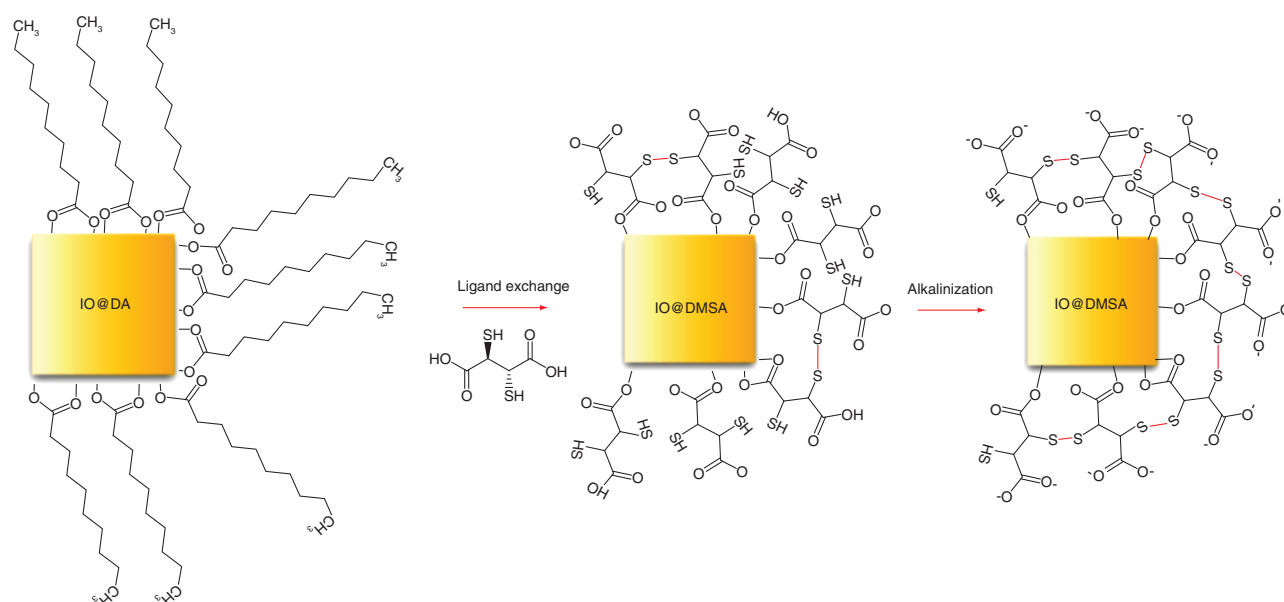


**Figure 8.** Schematic illustration of surface modified iron oxide nanoparticles with monodentate and bidentate ligand bonds. The phase transfer reaction was performed through the reaction of DA-coated IO nanoparticles with DMSA. After ligand exchange reaction, alkalization (or deprotonization) of DMSA with 1 M KOH solution at pH 10 was performed to enhance the stability of the nanoparticles by electrostatic repulsion between COO<sup>-</sup> groups and by increasing S–S bonds to reduce hydrodynamic size. IO: Iron oxide; DA: Decanoic acid; DMSA: Meso-2,3-dimercaptosuccinic acid.

## Discussion

We described here DMSA-coated cubic IONPs that have been prepared by the ligand exchange of DA on the surface of the IONPs with DMSA. The aim of the study was to obtain biocompatible superparamagnetic cubic IONPs having the size just below the superparamagnetic size limit to get the NPs having high magnetization and good magnetothermal property for potential application as therapeutic agent. NPs have been investigated on their magnetothermal (hyperthermia) property and cytotoxicity of incubated NPs on HeLa cells was also carried out. This study appears to be the first study to investigate both hyperthermia property and *in vitro* cytotoxicity of DMSA-coated cubic IONPs on HeLa cells.

The modifications in the IONP synthesis procedure, such as using different surfactant amount and different heating rate, resulted in superparamagnetic property of the obtained IONPs unlike the ferromagnetic one in the study of Guardia *et al.* [32] where IONPs were transferred to polar solvents using a different surfactant (gallic acid-polyethylene glycol).

To assess the percentages of the magnetic and organic masses, TGA analyses were performed. The TGA curves were also used to predict the layer and bonding structures of the surfactant molecules on the NP surface. The three desorption processes in TGA curves of DA- and DMSA-coated IONPs (Figure 4Aa & 4Ab) can be explained by the two possible scenarios: first, a bilayer structure or, second, two kinds of bonding (monodentate and bidentate) structures of the surfactant molecules on the NP surface.

In the first scenario [38,43,44], it is assumed that there are DA/DMSA bilayers on the NP surface, due to chemisorption and physisorption of these ligands. While the mass loss at highest temperature could be due to strong binding between the inner layer of ligands and IONPs, the one at the lower temperature arises from the removal of the outer layer of ligands on the NPs that bind weakly to the first layer. The third mass loss at the lowest temperature, which is ~210°C, might arise from the residual ligands weakly physisorbed on the NP surface.

For the second scenario [36], it is assumed that there is a single coating layer adsorbed on the NP surface and that these two mass losses at two different temperatures arise from the two types of bonding pattern of the ligands – monodentate and bidentate bonding – meaning that they have different bond strengths. A schematic illustration for DMSA-coated IONPs with monodentate and bidentate ligand bonds is given in Figure 8. The third mass loss

may also be attributed to the residual ligands adsorbed on the surface. The different paths of the curve a and curve b (Figure 4A) is due to different amounts of coating materials on the surface of the NPs.

We observed significant improvement of the magnetic property of the IONPs after DMSA functionalization while keeping their superparamagnetic property. The improvement in the saturation magnetization of the IONPs after ligand exchange can be attributed to the different functional groups bounded to the particle surfaces causing different interactions between the ligands and Fe atoms, and it alters the surface magnetic state of the NPs. Different shell type shields the magnetic core differently depending on its magnetic permeability, electron transfer ability and structural stability [45]. The increase in the saturation magnetization of IONPs after ligand exchange with DMSA is somewhat similar to that reported previously for the oleic acid coated  $\text{Fe}_3\text{O}_4$  NPs [46,47]. It is also known that DMSA molecule has short chain and lower molecular weight in comparison with DA. It is expected that DMSA cause less magnetic shielding effect on the IONPs. In addition, establishing interparticle disulfide bonds can also contribute to shortening the distance between the magnetic cores of the NPs and result in increased magnetic interactions. Therefore, DMSA-coated IONPs are expected to have higher magnetization than DA-coated IONPs.

XRD pattern of the IONPs before the ligand exchange with DMSA showed no signs of wüstite presence (see Supplementary Figure 3), the improvement of magnetization value of the NPs after the ligand exchange process therefore cannot be attributed to the contribution of the oxidation of the nonmagnetic wüstite phase to the ferrimagnetic magnetite in the presence of water during the ligand exchange with DMSA. Hence, XRD pattern of DMSA coated NPs was not important to study.

Compared with previous studies, magnetic saturation value of 24.5 nm nanocubes at room temperature ( $M_s = 74.2 \text{ emu g}^{-1}$  for DA-coated IONPs,  $M_s = 89.6 \text{ emu g}^{-1}$  for DMSA-coated IONPs) is much higher than those reported for 27 nm nanocubes ( $<60 \text{ emu g}^{-1}$  for Fe) [24]; for 10 nm spherical NPs ( $50 \text{ emu g}^{-1}$  for both DMSA-coated and uncoated IONPs) [20]; for 10 nm spherical NPs ( $70 \text{ emu g}^{-1}$  for IONPs) [21]; for 12 nm nanocubes ( $69 \text{ emu g}^{-1}$  for IONPs) [25]; for 14-18 nm nanocubes ( $<70 \text{ emu g}^{-1}$  for DMSA-coated IONPs) [27], which can be attributed to higher magnetic core size and better crystallinity. The results indicate that the NPs reported in this article can have potential biomedical applications, such as hyperthermia therapy. The other studies have not been reported magnetization value of their NPs [48] or did not perform the magnetic characterization of NPs [23].

The result of the hyperthermia experiment of DMSA-coated IONPs was promising, with a temperature rise of  $15^\circ\text{C}$  in  $\sim 5$  min under AMF. The obtained ILP value ( $1.59 \text{ nHm}^2\text{kg}^{-1}$ ) is larger than that of commercial 15.2 nm DMSA-coated  $\text{Fe}_3\text{O}_4$  (HyperMAG $^{\text{R}}\text{C}$ ) with reported SAR values of  $31 \text{ W/g}$  (AMF of  $18.6 \text{ kA/m}$  and frequency  $532 \text{ kHz}$ ,  $\text{ILP} = 0.17 \text{ nHm}^2\text{kg}^{-1}$ ) and  $48 \text{ W/g}$  (AMF of  $17.9 \text{ kA/m}$  and frequency  $267 \text{ kHz}$ ,  $\text{ILP} = 0.56 \text{ nHm}^2\text{kg}^{-1}$ ) [22]. Also, it is larger than that of the reported study of 18 nm DMSA-coated cubic IONPs (reported SAR value to be  $97 \text{ W/g}$ , AMF of  $39.9 \text{ kA/m}$  and frequency  $77 \text{ kHz}$ , calculated  $\text{ILP} = 0.79 \text{ nHm}^2\text{kg}^{-1}$ ) [27].

Potential effects of the DMSA-coated cubic IONPs on HeLa cells were investigated by MTT assay. The cytotoxicity results of DMSA-coated IONPs are in agreement with previous studies where the NPs with similar properties were studied for 24 h on HeLa cells [14,20,21,48]. In this study, the cells were incubated for longer time periods (48 and 72 h) without significant reduction of cell viability (above 78%). It was reported that superparamagnetic IONPs itself did not disturb basic cellular functions [12]. Our DMSA-coated IONPs did not show a time- or concentration-dependent cell viability of tested concentrations similar to earlier report on HeLa cells for 24 h [24]. A decrease in the cell viability is expected with increased concentration and incubation time of the IONPs [49]. However, the reason for the improved cell viability after a certain time of incubation with NPs may be originated from the released iron ions from the IONPs. It has been revealed that DMSA-coated  $\text{Fe}_3\text{O}_4$  NPs could degrade into iron ions in lysosomes [49]. Although the high amount of iron can produce reactive oxygen species (such as superoxide, hydroxyl radical and hydrogen peroxide) and thus causes cell toxicity; however, the low amount of iron is necessary for cell proliferation and essential for numerous metabolic pathways. The abundance of the iron in the medium might have caused an increase in cell viability. A similar result for the iron oxide nanorods has also been reported [50]. Performing filtration before cell culture experiments limited the range of concentrations to be tested in our study.

## Conclusion

We synthesized superparamagnetic DMSA-coated cubic IONPs with a hydrodynamic size less than 100 nm and a SAR value of  $197.4 \text{ W/g}_{\text{Fe}}$ . The saturation magnetization of the IONPs was increased after functionalization with DMSA which was attributed either to the bonding of functional groups with surface spin disorder or magnetic



shielding effects. The water-dispersible DMSA-coated IONPs slightly altered HeLa cell viability at the tested concentrations for the time periods of 24, 48 and 72 h and compared with the control groups. From the results of the study, the synthesized DMSA-coated IONPs can be a good candidate to be used as nontoxic therapeutic agents with the possibility of MRI imaging in biomedical application.

### Future perspective

It is predicted that superparamagnetic IONPs can make great contributions to human health in the future with their use as multifunctional theranostic agents in multimodal imaging and therapies. It is possible that the knowledge gained in this study may contribute to the development of further strategies on DMSA functionalized cubic IONPs, such as labeling with radioisotope or functionalization with a cancer-specific ligand for cancer diagnosis and treatment. *In vitro* assessment and analysis of cellular responses by the exposure of AMF should be investigated in future studies.

### Summary points

- This work details the preparation of meso-2,3-dimercaptosuccinic acid (DMSA) functionalized cubic superparamagnetic iron oxide nanoparticles (IONPs; IO@DMSA), which have a high potential use for multifunctional cancer diagnosis and treatment.
- The hydrodynamic sizes of the DMSA-coated IONPs were significantly reduced and the stability of them was greatly enhanced by alkalization step.
- IO@DMSA NPs possess good colloidal stability at physiological pH values and have a hydrodynamic size less than 100 nm, which is critical value to avoid rapid clearance of NPs through kidneys and reticuloendothelial system and to provide them prolonged blood circulation half-life.
- XRD confirms the presence of iron oxide with a reverse spinel structure and VSM result confirm that the DMSA-functionalized IONPs are superparamagnetic and that ligand exchange with DMSA resulted in an increase in the magnetic properties of the NPs, while keeping their superparamagnetic behavior.
- The result of the hyperthermia experiment for the cubic IONPs was promising, with a temperature rise of 15 °C in ~5 min under the tested magnetic field and frequency.
- IO@DMSA NPs have slight cytotoxic effect on HeLa cell viability at the concentrations studied up to 3 days compared with the control groups.
- This study appears to be the first to investigate both *in vitro* cytotoxicity of DMSA-coated cubic IONPs on HeLa cells and hyperthermia performance of these NPs.
- The results show a promising potential on the use of the cubic IONPs functionalized with DMSA for biomedical applications.

### Supplementary data

To view the supplementary data that accompany this paper please visit the journal website at: [www.futuremedicine.com/doi/suppl/10.2217/nnm-2020-0467](http://www.futuremedicine.com/doi/suppl/10.2217/nnm-2020-0467)

### Author contributions

S Çitoğlu was responsible for the design, synthesis, analysis and evaluation of the work reported in this study. She wrote the first draft of the manuscript. MA Onur designed and supervised the cytotoxicity experiments and contributed to the study with his helpful discussions. He provided feedback for the manuscript. LD Tung and NTK Thanh conducted and supervised the hyperthermia experiment. LD Tung provided revisions to the manuscript. NTK Thanh played a crucial role in analyzing the data and in critical revision of the manuscript. ÖD Coşkun is the PhD thesis supervisor and provided funding access to crucial research components (equipment and chemicals).

### Acknowledgments

This study has been performed for the PhD thesis of S Çitoğlu, who thanks Assoc. Prof. Aylin Özer Gürpınar for sharing her valuable knowledge on cell culture studies and Dr. Handan Sevim for her help during the preliminary works of the cell culture experiments. S Çitoğlu, ÖD Coşkun and MA Onur acknowledge the National Nanotechnology Research Center (UNAM) and Hacettepe University Advanced Technologies Application and Research Center (HÜNİTEK).

### Financial & competing interests disclosure

S Çitoğlu gratefully thanks The Scientific and Technological Research Council of Turkey – Directorate of Science Fellowships and Grant Programmes (TÜBİTAK-BİDEB) for supporting this research with 2211-C National PhD Scholarship Program for Priority Areas. This work was also supported in part by Hacettepe University Scientific Research Project (BAP) Coordination Unit, Turkey (Project No:

FHD-2018-16742). NTKT thanks EPSRC (EP/M015157/1 and EP/M018016/1); AOARD (FA2386-17-1-4042 award). The authors have no other relevant affiliations or financial involvement with any organization or entity with a financial interest in or financial conflict with the subject matter or materials discussed in the manuscript apart from those disclosed.

No writing assistance was utilized in the production of this manuscript.

### Open access

This work is licensed under the Creative Commons Attribution 4.0 License. To view a copy of this license, visit <http://creativecommons.org/licenses/by/4.0/>

## References

Papers of special note have been highlighted as: ● of interest

- Xie W, Guo Z, Gao F *et al.* Shape-, size- and structure-controlled synthesis and biocompatibility of iron oxide nanoparticles for magnetic theranostics. *Theranostics* 8(12), 3284–3307 (2018).
- **A review providing a background on the controlled synthesis, biocompatibility evaluation and applications of iron oxide nanoparticles as cancer theranostic agents.**
- Colombo M, Carregal-Romero S, Casula MF *et al.* Biological applications of magnetic nanoparticles. *Chem. Soc. Rev.* 41(11), 4306–4334 (2012).
- Ruiz A, Morais PC, de Azevedo RB *et al.* Magnetic nanoparticles coated with dimercaptosuccinic acid: development, characterization, and application in biomedicine. *J. Nanoparticle Res.* 16(2589), 1–20 (2014).
- **A review on DMSA-coated magnetic nanoparticles and their promising biomedical applications.**
- Wahajuddin, Arora S. Superparamagnetic iron oxide nanoparticles: magnetic nanoplatforms as drug carriers. *Int. J. Nanomedicine* 7, 3445–3471 (2012).
- Kumar CSSR, Mohammad F. Magnetic nanomaterials for hyperthermia-based therapy and controlled drug delivery. *Adv. Drug Deliv. Rev.* 63(9), 789–808 (2011).
- Stephen ZR, Kievit FM, Zhang M. Magnetite nanoparticles for medical MR imaging. *Mater. Today* 14(7–8), 330–338 (2011).
- Singh A, Sahoo SK. Magnetic nanoparticles: a novel platform for cancer theranostics. *Drug Discov. Today* 19(4), 474–481 (2014).
- Dadfar SM, Roemhild K, Drude NI *et al.* Iron oxide nanoparticles: diagnostic, therapeutic and theranostic applications. *Adv. Drug Deliv. Rev.* 138, 302–325 (2019).
- Lombardo D, Kiselev MA, Caccamo MT. Smart nanoparticles for drug delivery application: development of versatile nanocarrier platforms in biotechnology and nanomedicine. *J. Nanomater.* 2019, 3702518 (2019).
- Dulinska-Litewka J, Lazarczyk A, Halubiec P *et al.* Superparamagnetic iron oxide nanoparticles-current and prospective medical applications. *Mater. (Basel)* 12(4), 617 (2019).
- Shah A, Dobrovolskaia MA. Immunological effects of iron oxide nanoparticles and iron-based complex drug formulations: therapeutic benefits, toxicity, mechanistic insights, and translational considerations. *Nanomedicine* 14(3), 977–990 (2018).
- Wierzbinski KR, Szymanski T, Rozwadowska N *et al.* Potential use of superparamagnetic iron oxide nanoparticles for in vitro and in vivo bioimaging of human myoblasts. *Sci. Rep.* 8(1), 3682 (2018).
- **An article detailing biological impact of DMSA-coated spherical iron oxide nanoparticles on human skeletal myoblasts.**
- Palma SICJ, Marciello M, Carvalho A *et al.* Effects of phase transfer ligands on monodisperse iron oxide magnetic nanoparticles. *J. Colloid Interface Sci.* 437, 147–155 (2015).
- **An article evaluating the effects of surface coating with DMSA on the colloidal and magnetic properties of spherical iron oxide nanoparticles.**
- Calero M, Gutierrez L, Salas G *et al.* Efficient and safe internalization of magnetic iron oxide nanoparticles: two fundamental requirements for biomedical applications. *Nanomedicine* 10(4), 733–743 (2014).
- **An article assessing the safety associated with nanoparticles-cell interaction of three coating iron oxide nanoparticles on HeLa cells, including DMSA-coated spherical nanoparticles.**
- Mejias R, Perez-Yague S, Gutierrez L *et al.* Dimercaptosuccinic acid-coated magnetite nanoparticles for magnetically guided *in vivo* delivery of interferon gamma for cancer immunotherapy. *Biomaterials* 32(11), 2938–2952 (2011).
- **An article detailing DMSA-coated spherical magnetite nanoparticles as a delivery system for tumor immunotherapy.**
- Mejias R, Perez-Yague S, Roca AG *et al.* Liver and brain imaging through dimercaptosuccinic acid-coated iron oxide nanoparticles. *Nanomedicine (Lond.)* 5(3), 397–408 (2010).
- Cha Y, Kim M, Choa Y *et al.* Synthesis and characterizations of surface-coated superparamagnetic magnetite nanoparticles. *IEEE Trans. Magn.* 46(2), 443–446 (2010).
- **An article investigating the DMSA surface-modification effects on magnetite nanoparticles.**

18. Villanueva A, Canete M, Roca AG *et al.* The influence of surface functionalization on the enhanced internalization of magnetic nanoparticles in cancer cells. *Nanotechnology* 20(11), 115103 (2009).
19. Barick KC, Aslam M, Lin Y-P, Bahadur D, Prasad PV, Dravid VP. Novel and efficient MR active aqueous colloidal Fe<sub>3</sub>O<sub>4</sub> nanoassemblies. *J. Mater. Chem.* 19(38), 7023–7029 (2009).
20. Xiong F, Zhu Z, Xiong C *et al.* Preparation, characterization of 2-deoxy-D-glucose functionalized dimercaptosuccinic acid-coated maghemite nanoparticles for targeting tumor cells. *Pharm. Res.* 29(4), 1087–1097 (2012).
21. Ruiz A, Salas G, Calero M *et al.* Short-chain PEG molecules strongly bound to magnetic nanoparticle for MRI long circulating agents. *Acta Biomater.* 9(5), 6421–6430 (2013).
22. Gas P, Miskowski A. Specifying the ferrofluid parameters important from the viewpoint of magnetic fluid hyperthermia. Presented at: *2015 Selected Problems of Electrical Engineering and Electronics (WZEE)*. Kielce, Poland, (2015).
23. Monge-Fuentes V, Garcia MP, Tavares MCH *et al.* Biodistribution and biocompatibility of DMSA-stabilized maghemite magnetic nanoparticles in nonhuman primates (*Cebus* spp.). *Nanomedicine (Lond)*. 6(9), 1529–1544 (2011).
24. Pardo A, Pujales R, Blanco M *et al.* Analysis of the influence of synthetic parameters on the structure and physico-chemical properties of non-spherical iron oxide nanocrystals and their biological stability and compatibility. *Dalt. Trans.* 45(2), 797–810 (2016).
25. Cabrera LI, Somoza Á, Marco JF *et al.* Synthesis and surface modification of uniform MFe<sub>2</sub>O<sub>4</sub> (M = Fe, Mn, and Co) nanoparticles with tunable sizes and functionalities. *J. Nanoparticle Res.* 14(6), 873 (2012).
26. Kossatz S, Ludwig R, Dahring H *et al.* High therapeutic efficiency of magnetic hyperthermia in xenograft models achieved with moderate temperature dosages in the tumor area. *Pharm. Res.* 31(12), 3274–3288 (2014).
27. Salas G, Casado C, Teran FJ *et al.* Controlled synthesis of uniform magnetite nanocrystals with high-quality properties for biomedical applications. *J. Mater. Chem.* 22(39), 21065–21075 (2012).
- **An article investigating the influence of the size and size distribution on the magnetic and magneto-thermal properties of DMSA-coated spherical and cubic iron oxide nanoparticles.**
28. Martinez-Boubeta C, Simeonidis K, Makridis A *et al.* Learning from nature to improve the heat generation of iron-oxide nanoparticles for magnetic hyperthermia applications. *Sci. Rep.* 3(1), 1652 (2013).
29. Zhen G, Muir BW, Moffat BA *et al.* Comparative study of the magnetic behavior of spherical and cubic superparamagnetic iron oxide nanoparticles. 115, 327–334 (2011).
30. Veisoh O, Gunn JW, Zhang M. Design and fabrication of magnetic nanoparticles for targeted drug delivery and imaging. *Adv. Drug Deliv. Rev.* 62(3), 284–304 (2010).
31. Salatin S, Maleki Dizaj S, Yari Khosroushahi A. Effect of the surface modification, size, and shape on cellular uptake of nanoparticles. *Cell Biol. Int.* 39(8), 881–890 (2015).
32. Zhang L, Wang X, Zou J *et al.* DMSA-coated iron oxide nanoparticles greatly affect the expression of genes coding cysteine-rich proteins by their DMSA coating. *Chem. Res. Toxicol.* 28(10), 1961–1974 (2015).
33. Tsoukalas C, Psimadas D, Kastis GA *et al.* A novel metal-based imaging probe for targeted dual-modality SPECT/MR imaging of angiogenesis. *Front. Chem.* 6, 224 (2018).
34. Guardia P, Riedinger A, Nitti S *et al.* One pot synthesis of monodisperse water soluble iron oxide nanocrystals with high values of the specific absorption rate. *J. Mater. Chem. B* 2(28), 4426–4434 (2014).
35. Bloemen M, Brullot W, Luong TT *et al.* Improved functionalization of oleic acid-coated iron oxide nanoparticles for biomedical applications. *J. Nanopart. Res.* 14(9), 1100 (2012).
36. Zhang L, He R, Gu H-C. Oleic acid coating on the monodisperse magnetite nanoparticles. *Appl. Surf. Sci.* 253(5), 2611–2617 (2006).
37. Mahdavi M, Ahmad M Bin, Haron MJ *et al.* Synthesis, surface modification and characterisation of biocompatible magnetic iron oxide nanoparticles for biomedical applications. *Molecules* 18(7), 7533–7548 (2013).
38. De Palma R, Peeters S, Van Bael MJ *et al.* Silane ligand exchange to make hydrophobic superparamagnetic nanoparticles water-dispersible. *Chem. Mater.* 19(7), 1821–1831 (2007).
39. Zhang S, Chen X, Gu C *et al.* The effect of iron oxide magnetic nanoparticles on smooth muscle cells. *Nanoscale Res. Lett.* 4(1), 70 (2008).
40. Valois CRA, Braz JM, Nunes ES *et al.* The effect of DMSA-functionalized magnetic nanoparticles on transendothelial migration of monocytes in the murine lung via a beta2 integrin-dependent pathway. *Biomaterials* 31(2), 366–374 (2010).
41. Zaitsev VS, Filimonov DS, Presnyakov IA *et al.* Physical and chemical properties of magnetite and magnetite-polymer nanoparticles and their colloidal dispersions. *J. Colloid Interface Sci.* 212(1), 49–57 (1999).
42. Westrum EF, Grønvd F. Magnetite (Fe<sub>3</sub>O<sub>4</sub>) Heat capacity and thermodynamic properties from 5 to 350 K, low-temperature transition. *J. Chem. Thermodyn.* 1(6), 543–557 (1969).
43. Soares PIP, Laia CAT, Carvalho A *et al.* Iron oxide nanoparticles stabilized with a bilayer of oleic acid for magnetic hyperthermia and MRI applications. *Appl. Surf. Sci.* 383, 240–247 (2016).

44. Baharuddin AA, Ang BC, Abu Hussein NA *et al.* Mechanisms of highly stabilized ex-situ oleic acid-modified iron oxide nanoparticles functionalized with 4-pentynoic acid. *Mater. Chem. Phys.* 203, 212–222 (2018).
45. Zhang W, Chen J, Wang W *et al.* Super-paramagnetic core-shell material with tunable magnetic behavior by regulating electron transfer efficiency and structure stability of the shell. *Results Phys.* 6, 606–613 (2016).
46. Nagesha DK, Plouffe BD, Phan M *et al.* Functionalization-induced improvement in magnetic properties of Fe<sub>3</sub>O<sub>4</sub> nanoparticles for biomedical applications. *J. Appl. Phys.* 105(7), 07B317 (2009).
47. Woo K, Hong J, Ahn J-P. Synthesis and surface modification of hydrophobic magnetite to processible magnetite@silica-propylamine. *J. Magn. Magn. Mater.* 293(1), 177–181 (2005).
48. Tharkeshwar AK, Trekker J, Vermeire W *et al.* A novel approach to analyze lysosomal dysfunctions through subcellular proteomics and lipidomics: the case of NPC1 deficiency. *Sci. Rep.* 7, 41408 (2017).
49. Liu Y, Wang J. Effects of DMSA-coated Fe<sub>3</sub>O<sub>4</sub> nanoparticles on the transcription of genes related to iron and osmosis homeostasis. *Toxicol. Sci.* 131(2), 521–536 (2012).
50. Ghasempour S, Shokrgozar MA, Ghasempour R, Alipour M. Investigating the cytotoxicity of iron oxide nanoparticles in in vivo and in vitro studies. *Exp. Toxicol. Pathol.* 67(10), 509–515 (2015).

